Loop Current Order on the Kagome Lattice

Jun Zhan,[1,2,*] Hendrik Hohmann,[3,*] Matteo Dürrnagel,[3,4] Ruiqing Fu,[5,2] Sen Zhou,[5] Ziqiang Wang,[6] Ronny Thomale,[3] Xianxin Wu,[5,†] and Jiangping Hu[1,2,7,‡]

[1]*Beijing National Laboratory for Condensed Matter Physics and Institute of Physics, Chinese Academy of Sciences, Beijing 100190, China*

[2]*School of Physical Sciences, University of Chinese Academy of Sciences, Beijing 100049, China*

[3]*Institut für Theoretische Physik und Astrophysik, Universität Würzburg, Am Hubland Campus Süd, Würzburg 97074, Germany*

[4]*Institute for Theoretical Physics, ETH Zürich, 8093 Zürich, Switzerland*

[5]*Institute of Theoretical Physics, Chinese Academy of Sciences, Beijing 100190, China*

[6]*Department of Physics, Boston College, Chestnut Hill, Massachusetts 02467, USA*

[7]*New Cornerstone Science Laboratory, Institute of Physics, Chinese Academy of Sciences, Beijing 100190, China*

(Received 16 October 2024; accepted 25 February 2026; published 25 March 2026)

Recent discoveries in kagome materials have unveiled their capacity to harbor exotic quantum states, including intriguing charge density wave (CDW) and superconductivity. Notably, accumulating experimental evidence suggests time-reversal symmetry breaking within the CDW, hinting at the long-pursued loop current order (LCO). Despite extensive research efforts, achieving its model realization and understanding the mechanism through unbiased many-body simulations have remained both elusive and challenging. In this Letter, we develop a microscopic model for LCO on the spinless kagome lattice with nonlocal interactions, utilizing unbiased functional renormalization group calculations to explore ordering tendencies across all two-particle scattering channels. At the Van Hove filling, we identify sublattice interference to suppress onsite CDW order, leaving LCO, charge bond order, and nematic CDW state as the main competitors. Remarkably, a 2×2 LCO emerges as the many-body ground state over a significant parameter space with strong second nearest-neighbor repulsion, stemming from the unique interplay between sublattice characters and lattice geometry. The resulting electronic model with LCO bears similarities to the Haldane model and culminates in a quantum anomalous Hall state. We also discuss potential experimental implications for kagome metals.

DOI: 10.1103/5vyy-rj6v

Magnetic transition-metal based kagome materials, consisting of corner-sharing triangles, present an exciting platform to explore intriguing correlated and topological phenomena, including quantum spin liquid [1–3], Dirac and Weyl semimetals [4–6]. They arise from the inherent features of the kagome lattice, including substantial geometric spin frustration, flat bands and Dirac cones. However, despite theoretical studies that have spanned over a decade, the exploration of Van Hove singularities (VHS), another critical feature of kagome lattices, has been hampered experimentally by the scarcity of suitable materials. Consequently, the recent discovery of kagome metals that feature VHS in the vicinity of the Fermi level, leading to the emergence of diverse quantum states such as superconductivity, charge density wave (CDW) order and nematicity, have garnered significant attention. In particular, the CDW in AV_3Sb_5 (A = K,Rb,Cs) [7–9] and FeGe [10–13] has been found to exhibit intriguing properties. In AV_3Sb_5, a CDW transition occurs below $T_{CDW} = 78$–103 K, characterized by a breaking of translational symmetry, resulting in either a $2 \times 2 \times 2$ or $2 \times 2 \times 4$ configuration. Intriguingly, various measurements, such as muon spin resonance (μSR) [14,15] and magneto-optical Kerr effect experiments [16–19], have provided evidence of time-reversal symmetry (TRS) breaking within the CDW in the absence of magnetic ordering. Superconductivity subsequently emerges within the CDW phase, reaching a maximum T_c of 2.5 K at ambient pressure, with double superconducting domes observed under pressure and doping [20–25]. In the antiferromagnet FeGe with ferromagnetic kagome layers, a CDW order occurs below the magnetic transition temperature [10]. The CDW exhibits topological characters with a $2 \times 2 \times 2$ reconstruction and an enhancement in the magnetic moment and anomalous Hall effect are observed upon the CDW transition [11,13]. This experimental evidence indicates the occurrence of long-pursued loop current order (LCO) within the kagome lattice [26–29], reminiscent of flux states suggested in cuprates [30–32] and Haldane model [33].

*These authors contributed equally to this work.

†Contact author: xxwu@itp.ac.cn

‡Contact author: jphu@iphy.ac.cn

The concept of a current-carrying phase, a rare state of matter, has been proposed in the pseudogap phase of cuprate and honeycomb systems through phenomenological or mean-field analyses [30–34]. Whether this loop current phase could serve as a precursor or parent state to exotic quantum phenomena like high-T_c superconductivity and quantum anomalous Hall effect has long been debated. However, the experimental verification of LCO in cuprate and its theoretical stability beyond mean-field level in square and honeycomb lattice remains controversial. Unbiased many-body calculations have indicated that the true ground state is not LCO but onsite charge or spin order under conventional interaction settings [35–44]. This has relegated LCO to a phenomenological hypothesis rather than a microscopic reality. However, various TRS breaking evidence within CDW of kagome metals offers strong motivation to explore the possibility of LCO in the kagome lattice. The VHS of the kagome lattice exhibit unique sublattice texture on the Fermi surface (FS) [45,46], which significantly impacts the electronic instabilities. Importantly, the implied sublattice interference effect suppresses local interaction scales, thereby enhancing the role of the long-range tail of the screened Coulomb repulsion [47–49]. Nevertheless, prior studies have shown the absence of LCO in simple interacting kagome models, rendering its realization challenging [47–50]. Recent theoretical analyses imply that long-range interactions and frozen spin degrees of freedom may promote LCO [51,52]. Therefore, whether the simple kagome lattice can realize LCO as the many-body ground state and what the microscopic mechanism entails are outstanding questions. This necessitates an unbiased many-body investigation that adequately accounts for competing fluctuations in all channels.

Motivated by these fundamental questions, we concentrate on the inherent CDW phenomena in the kagome lattice at Van Hove filling. We adopt the spinless kagome model with nonlocal interactions, which can avoid complex spin fluctuations and have direct experimental relevance to materials, like magnet FeGe, hosting spin-polarized low-energy electronic structures. To comprehensively address fluctuations across channels, we employ the unbiased functional renormalization group (FRG) approach to analyze FS instabilities. Our calculations reveal that the second nearest-neighbor repulsion can promote fluctuations of imaginary bond charge order, driven by the sublattice interference and frustrated kagome geometry. This results in a 2×2 LCO ground state, which prevails over a substantial parameter space when the second nearest-neighbor repulsion is notably strong. Remarkably, this TRS breaking 2×2 LCO is validated for the first time, to our knowledge, as the many-body ground state through rigorous many-body calculations, confirming its existence in the kagome lattice. We also observe the nematic CDW, charge bond order, and f-wave superconductivity (SC) for different parameters, which are potentially relevant for kagome metals.

Interacting kagome model and formalism of FRG—To explore the intrinsic charge orders driven by electronic interactions within the kagome lattice, we study the model under a spinless scenario that involves density-density interactions. The full Hamiltonian including kinetic energy and nonlocal interactions reads

$$H = -t\sum_{\langle i,j\rangle}(c_i^\dagger c_j + \text{H.c.}) - \mu\sum_i n_i + V_1\sum_{\langle i,j\rangle} n_i n_j + V_2\sum_{\langle\langle i,j\rangle\rangle} n_i n_j, \tag{1}$$

where $c_i^\dagger$ creates an electron on lattice site i, t is the nearest-neighbor hopping amplitude, $n_i = c_i^\dagger c_i$ is the electron density operator which couples to the chemical potential μ, and V_n is the n th nearest-neighbor ($n$nn) Coulomb repulsion. Distinct from the spinful case, the spin degrees of freedom are frozen here, and the onsite interaction is absent in Eq. (1) as fermionic antisymmetry precludes double occupation of a single site [52,53]. The single-particle dispersion features a flat band, Dirac cones and two different kinds of VHS, which are characterized by distinct sublattice texture on the FS [46,47], distinct from triangular and honeycomb lattices. In this Letter we focus on the p-type VHS with $\mu = 0$, where each inequivalent M point consists of states solely attributed to one sublattice, and the nesting vectors $\boldsymbol{Q}_{A,B,C}$ connect saddle points with distinct sublattice characters [see Supplemental Material (SM) [54]].

To properly address the intricate competition between many-body correlated states within the interacting kagome model, we employ FRG calculations, which take into account all intertwined particle-hole and particle-particle fluctuations on equal footing [62–64]. The leading instability is extracted by the eigenvector associated with the most divergent eigenvalue of the effective vertex function at Λ_c, where FRG flow exhibits a divergence. To monitor the propensity of the system toward various symmetry broken states $|\Phi_\theta\rangle$ within the FRG flow, we determine the expectation value $\Xi = \langle\Phi_\theta|V_\Lambda|\Phi_\theta\rangle$ of the effective FRG vertex V at each flow step. The detailed descriptions of the FRG formalism and the implementation are provided in SM [54].

Intrinsic bond order fluctuations—In the triangular and honeycomb lattices with nonlocal Coulomb interactions, the dominant instability associated with VHS is the onsite CDW order at the nesting vectors [44,65,66], owing to its significant reduction of the potential energy of nonlocal repulsion. However, in the kagome lattice, onsite CDW fluctuations at the nesting vector are significantly suppressed due to the sublattice texture at Van Hove filling and the associated sublattice interference (SI) effect gives rise to a pronounced inclination toward bond charge orders [47,49,52]. The SI effect on charge states can be clearly

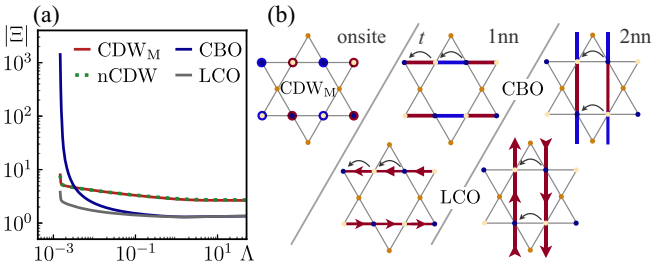

FIG. 1. Representative FRG flow with 1nn repulsion and real-space CDW patterns. (a) FRG flow of the expectation values of CBO, LCO, nCDW, and $\mathrm{CDW_M}$ and for $V_1 = t$ and $V_2 = 0$. (b) Real-space configurations of CBO and LCO on 1nn and 2nn bond as well as the onsite modulated CDW with a wave vector of $\boldsymbol{Q}_C$. The real-space pattern at two other nesting vectors can be obtained by the application of sixfold rotational operation. Red (blue) denotes positive (negative) onsite or bond order parameters, while arrows denote directions of current flows. Only the bond orders within the antisymmetric channel are depicted.

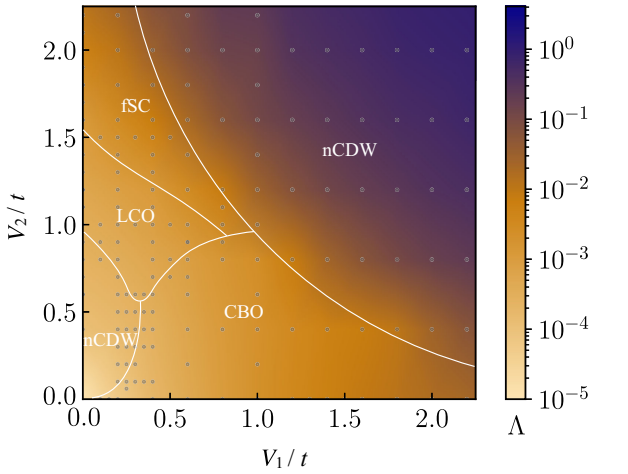

FIG. 2. Phase diagram of the spinless interacting kagome model at the p-type Van Hove filling. The critical scales Λ_c proportional to the expected transition temperature T_c are indicated by color. Gray dots indicate the calculated points in interaction parameter space.

demonstrated in the FRG flow with a typical nearest-neighbor repulsion $V_1 = t$ shown in Fig. 1(a). Starting from the bare interacting system at a high energy scale, *onsite* CDW fluctuations at $\boldsymbol{Q} = 0$ (nCDW) and $\boldsymbol{Q} = \mathrm{M}$ [$\mathrm{CDW_M}$, see Fig. 1(b)] are initially dominant, in accordance with other hexagonal lattice systems [45,65,66]. By successively integrating out the high-energy modes, the eigenvalue of charge bond orders [CBO, Fig. 1(b)] increases dramatically and eventually exceeds those of onsite CDW orders at an intermediate scale and finally diverges, indicating a leading instability of *real* charge bond order. Strikingly, this is accompanied by the emergence of a competing imaginary charge bond order. Figure 1(b) shows the real-space pattern of relevant onsite CDW, real and imaginary bond orders with the wave vector of $\boldsymbol{Q}_C$, where onsite charge and bond modulations are represented by different colors and the arrows denote the direction of currents.

FRG phase diagram—We conducted thorough FRG calculations for the model described in Eq. (1). The correlated phases identified within the interaction parameter space are depicted in Fig. 2, where the color represents the critical cutoff. In the regime of strong interactions, we recover a twofold nematic charge density wave (nCDW) as the classical solution of the interacting part of the Hamiltonian, that can acquire significant electrostatic energy gain by introducing unequal occupation between the three sublattices [52]. This energy gain is linear with respect to the nonlocal repulsion, leading to the nCDW becoming the dominant order with high critical scales at large repulsion. This twofold nCDW mainly involves an intraunit cell charge density wave. At lower scales, electronic screening effects dictate the realized phases: in the V_1 dominated regime, the system develops an instability toward CBO as known from prior studies of the spinful case [47,49,67]. Remarkably, we observe the emergence of a TRS breaking LCO state in the intermediate V_2 regime. This state is situated between regions of unconventional f-wave superconducting order in the strong V_2 regime and twofold nCDW in the weak V_2 regime. In the following, we will focus on the loop current order, elucidating both its underlying mechanism and physical properties of the symmetry broken state. In particular, we will identify the competition and cooperation between the different phases present in the V_2 dominated regime and address the apparent asymmetry to the CBO phase in the V_1 regime.

Loop current order—In the intermediate V_2 regime, the representative flows with LCO as leading instability are illustrated in Fig. 3(a) with $V_2 = 1.1t$ and $V_1 = 0$. The nCDW occurs as close competitor, distinct from the V_1 dominant case in Fig. 1(a). The observed LCO mainly involves a mixture between the 1nn and 2nn bonds from diagonalizing renormalized susceptibility, in contrast to dominant 1nn bond of loop current pattern reported in previous studies [51,68]. The inclusion of 1nn repulsion V_1 modifies real-space structure of LCO, which is evidenced by the changing weights of 1nn and 2nn bond orders along the parameter line $V_1 + V_2 = 1.2t$, as shown in Fig. 3(b). An increase in V_1 enhances the 1nn component in the LCO, which in turn significantly enhances the CBO due to pronounced 1nn real bond fluctuations and triggers a transition from LCO to CBO, where the 1nn and 2nn bond components exhibit a jump and drop, respectively. The LCO is dominant in a relatively large regime and is stabilized by stronger imaginary bond fluctuation on the 2nn bond compared to that in real bond channel, which is a direct consequence of the SI effect and unique kagome lattice geometry [52]. Intuitively, the intimate relation between the bond length and the prevalence of real or imaginary bond orders can be directly inferred from the different transformation behavior of LCO and CBO under

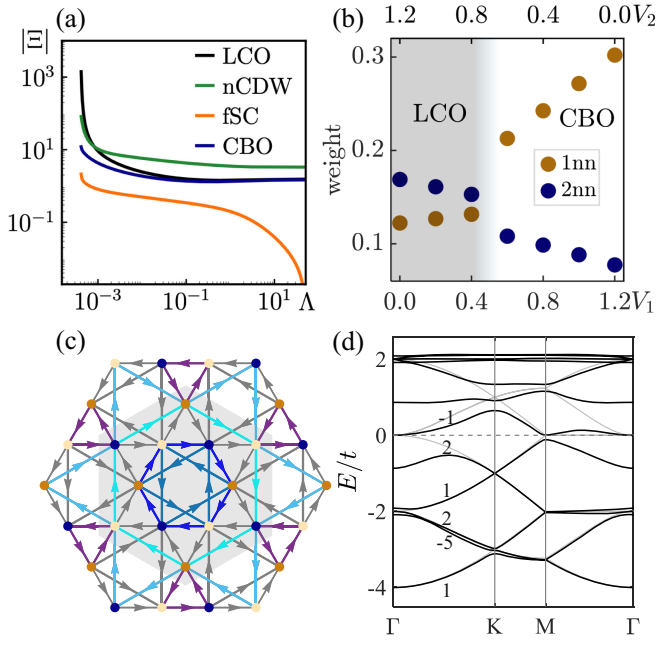

FIG. 3. (a) Representative FRG flow of the expectation values of nCDW, 2nn CBO, 2nn LCO, and fSC for $V_1 = 0$ and $V_2 = 1.1t$. (b) Variation of 1nn and 2nn contributions to the LCO and CBO phases as a function of changing V_1 and V_2 at fixed $V_1 + V_2 = 1.2t$. (c) Real-space pattern of the representative $3\boldsymbol{Q}$ LCO on both 1nn and 2nn bonds. The enlarged 2×2 supercell is indicated by gray shading. (d) Emergent Chern bands of the LCO phase in the folded BZ with order parameters $\Delta_{1\mathrm{nn}}^{\mathrm{LCO}} = 0.1t$ and $\Delta_{2\mathrm{nn}}^{\mathrm{LCO}} = 0.15t$, exhibiting a full gap around the Fermi level. The filled bands feature a total Chern number of $C = 1$. Gray curves indicate the backfolded dispersion.

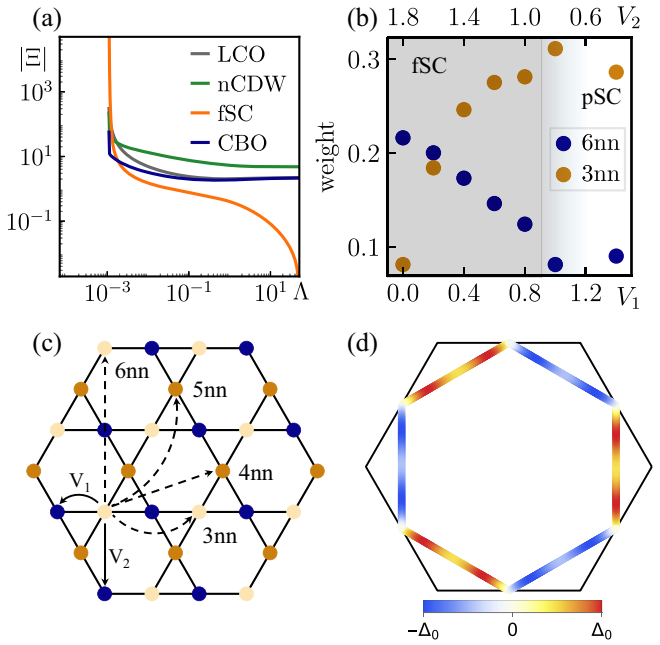

FIG. 4. (a) FRG flow of leading instabilities for $V_1 = 0$ and $V_2 = 1.6t$. (b) Variation of 3nn and 6nn components in the f- and p-wave superconductivity as a function of changing V_1 and V_2. (c) Schematics for the real-space pairing configuration, mediated by a combination of high-order virtual V_1 and V_2 processes. (d) f-wave gap function on the FS transforming under the B_{2u} representation in the V_2 dominant regime.

short range hopping fluctuations of particle-hole pairs, that result in an energy splitting already at second order in Ginzburg-Landau theory (details in Sec. III of SM [54]).

In accordance with the nesting vectors and sublattice makeup of the FS, the LCO establishes at the three inequivalent nesting vectors $\boldsymbol{Q}_{A,B,C}$, involving particle-hole pairs between three different bonds. To analyze the ground state, we minimize the Landau free energy containing three degenerate order parameters $\Delta_{1,2,3}$, each associated with one of the nesting vectors. In the Ginzburg-Landau expansion, their couplings at quartic order govern the ground state energy and are given by

$$f^{(4)} = \frac{1}{2} Z_1 |\boldsymbol{\Delta}|^4 + (Z_2 - Z_1)(\Delta_1^2 \Delta_2^2 + \Delta_2^2 \Delta_3^2 + \Delta_3^2 \Delta_1^2), \quad (2)$$

with $Z_1 - Z_2 > 0$ as explicated in the SM [54]. Different from the CBO case, the trilinear term vanishes owing to the TRS breaking. These quartic terms favor an equal contribution of the $3\boldsymbol{Q}$ modulations, leading to an enlarged 2×2 pattern. The characteristic pattern of the LCO maintaining the sixfold rotational symmetry is shown in Fig. 3(c), where currents of equal color form closed loops around the rotational center. This TRS breaking $3\boldsymbol{Q}$ LCO fully gaps out the FS and generates a Chern insulator, analogous to the Haldane model. This state features topologically nontrivial bands close to the Fermi level, as shown in Fig. 3(d), and Chern Fermi pockets can be introduced upon electron or hole doping.

Surprisingly, lowering the interaction scale triggers a transition from the LCO to a reentrant twofold CDW order at $\boldsymbol{q} = 0$, corresponding to the two dimensional E_{2g} representation of D_{6h}. The minimization of the free energy within the associated two dimensional eigenspace leads to a nematic order that breaks the sixfold rotational symmetry. There are three possible configurations with an unequal charge occupation of three sublattices, as shown in SM [54]. According to our analysis, the projection of particle-particle fluctuations onto the particle-hole channels promotes nCDW but simultaneously suppresses LCO (see Sec. VI of SM for more details [54]), rendering the nCDW slightly dominant.

f-wave superconductivity—For larger values of V_2 the LCO is surpassed by a superconducting instability mediated by the particle-hole fluctuations within LCO and nCDW channels [cf. Fig. 4(a)]. Caused by the spinless restriction, the pairing order parameter is odd in real space due to fermionic anti-commutation, which implies a vanishing gap at time reversal invariant momenta. Since the singular DOS at the M points cannot be gapped out by the superconducting order, SC phases are less prominent in the

phase diagram of Fig. 2 compared to prior studies on the spinful kagome lattice [49,67,69].

The remaining FS is fully gapped by an exotic f-wave SC order corresponding to the B_{2u} irreducible representation [cf. Fig. 4(c)]. In real space, this corresponds to Cooper pairing between 5th and 6th nn sites. In the $V_1 = 0$ case, these represent the closest sites available for pair formation mediated by the second order V_2 processes as indicated in Fig. 4(c). The sublattice texture on the Fermi surface favors Cooper pair formation on the 6nn compared to the 5nn bonds, since the states at $\mathbf{k}$ and $-\mathbf{k}$ near the VHS are mainly constituted by the same sublattice. Consequently, the intrasublattice pairing, like the 6nn bond, can gap out Fermi segments with high DOS, resulting in a significant condensation energy gain.

A sizable V_1 induces pairing between the 3nn sites due to mixed $V_1 - V_2$ processes as depicted in Fig. 4(b). The decreased distance between Cooper pairs reduces the gap modulation along the FS and increases the condensation energy gain by the SC order. A substantial V_1 leads to a transition from the f-wave to p-wave pairing symmetry in the particle-particle channel [Fig. 4(b)], which is subleading to the CBO in the V_1-dominant regime. The SC order can thereby exploit V_1 to gain energy opposed to the LCO, which exclusively relies on V_2 for its emergence [compare Figs. 4(a) and 3(b)]. Hence, the phase boundary to the SC state is shifted to lower V_2 values with increasing V_1, thereby bounding the LCO domain from above.

Discussion and conclusion—Our minimal model isolates the kagome-intrinsic ingredients that stabilize LCO—the interplay between VHS-related sublattice texture and lattice geometry—a mechanism that is generic to frustrated lattices (e.g., checkerboard, pyrochlore). The resulting sublattice interference effect not only promotes bond fluctuations at the nesting vectors but also impacts the superconducting pairing. In the spinful case, either superconductivity or nCDW is leading on the V_1 axis stemming from enhanced onsite CDW fluctuation at $\boldsymbol{q} = 0$, in contrast to the sole CBO in the spinless case [27,49]. The inclusion of V_2 in the spinful case yields a similar effect, making LCO subleading, as confirmed by our FRG calculations. Compensating for this overscreening by introducing the onsite repulsion U will suppress the CDW but a large U triggers magnetic orders as previously reported for $U \gg V_1$ [49,67].

We discuss experimental implications of our model calculations and identified mechanism for charge orders in kagome materials. The intriguing CDW in kagome metals FeGe and AV_3Sb_5 can be linked to instabilities associated with VHS, which have been identified in the vicinity of the Fermi level in ARPES measurements [11,12,70,71]. In these materials, strong d-p hybridization leads to delocalized d-orbital Wannier functions, resulting in comparable 1nn and 2nn Coulomb repulsion. Indeed, cRPA calculations find a ratio about $V_1/V_2 = 1.1$ [72], placing them near the boundary where LCO and CBO can coexist. Moreover, electron-phonon coupling [73,74] can generate an effective 1nn attraction which counteracts the repulsion V_1, potentially realizing an effective $V_2 > V_1$ regime. The multiorbital nature and multiple VHS in realistic materials may further enhance loop-current fluctuations and thus facilitate LCO formation. In FeGe, the large ferromagnetic splitting in each layer results in a spin-polarized p-type VHS in proximity to the Fermi level, analogous to our spinless model. Even when employing the spinful model with large ferromagnetic splitting to simulate FeGe, our FRG calculations reveal that LCO occurs with an intermediate 2nn repulsion, showing almost quantitative consistency with the spinless model (see SM [54]). According to our calculations, the 2×2 LCO in FeGe can generate an orbital magnetic moment as large as 0.03 μ_B per site, which may account for the observed magnetic moment change upon the CDW transition (details in SM [54]). For the multiorbital AV_3Sb_5, both p- and m-type VHS from the V-kagome net occur near the Fermi level [11,12]. Signatures of TRS breaking inside the CDW have been reported in different experimental measurements. The LCO, while subdominant in the single-orbital spinful model, may become stable in multiorbital AV_3Sb_5 through the combined effect of loop-current fluctuations amplification from distinct types of VHS [68,75] and reduced nn repulsion due to electron-phonon coupling [73,74]. The exotic interplay between LCO and superconductivity can generate intriguing pair density wave states [76].

Our Letter offers critical insights into intrinsic quantum fluctuations and their interplay with lattice geometry within the kagome lattice. By identifying 2×2 LCO through unbiased many-body calculations, we transform it from a speculative concept into a microscopically validated quantum state, establishing a solid theoretical foundation for the experimental exploration of LCO within kagome metals. This highlights the kagome metals as an ideal platform to study exotic correlated phenomena.

Acknowledgments—J. Z. and J. H. are supported by the Ministry of Science and Technology (Grant No. 2022YFA1403901), the National Natural Science Foundation of China (Grant No. 12494594) and the New Cornerstone Investigator Program. R. F., S. Z., and X. W. are supported by the National Key R&D Program of China (Grants No. 2023YFA1407300 and No. 2022YFA1403800) and the National Natural Science Foundation of China (Grants No. 12574151, No. 12447103, No. 12447101, No. 12374153, and No. 12047503). Z. W. is supported by U.S. Department of Energy, Basic Energy Sciences Grant No. DE-FG02-99ER45747 and the Cottrell SEED Award No. 27856 from Research Corporation for Science Advancement. M. D. is grateful for support from a Ph.D. scholarship of the Studienstiftung des deutschen Volkes. The work is funded by the Deutsche Forschungsgemeinschaft (DFG, German Research

Foundation) through Project No. 258499086–SFB 1170, and through the research unit QUAST, FOR 5249, Project No. 449872909, and through the Würzburg-Dresden Cluster of Excellence on Complexity and Topology in Quantum Matter–*ct.qmat* Project No. 390858490–EXC 2147. We acknowledge HPC resources provided by the Erlangen National High Performance Computing Center (NHR@FAU) of the Friedrich-Alexander-Universität Erlangen-Nürnberg (FAU). NHR funding is provided by federal and Bavarian state authorities. NHR@FAU hardware is partially funded by DFG Grant No. 440719683.

[1] M. R. Norman, Rev. Mod. Phys. **88**, 041002 (2016).
[2] A. Mielke, J. Phys. A **24**, L73 (1991).
[3] F. Pollmann, P. Fulde, and K. Shtengel, Phys. Rev. Lett. **100**, 136404 (2008).
[4] L. Ye, M. Kang, J. Liu, F. von Cube, C. R. Wicker, T. Suzuki, C. Jozwiak, A. Bostwick, E. Rotenberg, D. C. Bell, L. Fu, R. Comin, and J. G. Checkelsky, Nature (London) **555**, 638 (2018).
[5] J.-X. Yin *et al.*, Nature (London) **583**, 533 (2020).
[6] M. Kang *et al.*, Nat. Mater. **19**, 163 (2020).
[7] B. R. Ortiz, L. C. Gomes, J. R. Morey, M. Winiarski, M. Bordelon, J. S. Mangum, Iain W. H. Oswald, J. A. Rodriguez-Rivera, J. R. Neilson, S. D. Wilson, E. Ertekin, T. M. McQueen, and E. S. Toberer, Phys. Rev. Mater. **3**, 094407 (2019).
[8] T. Neupert, M. M. Denner, J.-X. Yin, R. Thomale, and M. Z. Hasan, Nat. Phys. **18**, 137 (2022).
[9] K. Jiang, T. Wu, J.-X. Yin, Z. Wang, M. Z. Hasan, S. D. Wilson, X. Chen, and J. Hu, Natl. Sci. Rev. **10**, nwac199 (2022).
[10] J.-X. Yin *et al.*, Phys. Rev. Lett. **129**, 166401 (2022).
[11] X. Teng *et al.*, Nature (London) **609**, 490 (2022).
[12] X. Teng, J. S. Oh, H. Tan, L. Chen, J. Huang, B. Gao, J.-X. Yin, J.-H. Chu, M. Hashimoto, D. Lu, C. Jozwiak, A. Bostwick, E. Rotenberg, G. E. Granroth, B. Yan, R. J. Birgeneau, P. Dai, and M. Yi, Nat. Phys. **19**, 814 (2023).
[13] S. Han, L. Li, C. S. Tang, Q. Wang, L. Zhang, C. Diao, M. Zhao, S. Sun, L. Tian, M. B. H. Breese, C. Cai, M. V. Milosevic, Y. Qi, A. T. S. Wee, and X. Yin, arXiv: 2407.01076.
[14] C. Mielke, D. Das, J. X. Yin, H. Liu, R. Gupta, Y. X. Jiang, M. Medarde, X. Wu, H. C. Lei, J. Chang, P. Dai, Q. Si, H. Miao, R. Thomale, T. Neupert, Y. Shi, R. Khasanov, M. Z. Hasan, H. Luetkens, and Z. Guguchia, Nature (London) **602**, 245 (2022).
[15] L. Yu, C. Wang, Y. Zhang, M. Sander, S. Ni, Z. Lu, S. Ma, Z. Wang, Z. Zhao, H. Chen, K. Jiang, Y. Zhang, H. Yang, F. Zhou, X. Dong, S. L. Johnson, M. J. Graf, J. Hu, H.-J. Gao, and Z. Zhao, arXiv:2107.10714.
[16] Q. Wu, Z. X. Wang, Q. M. Liu, R. S. Li, S. X. Xu, Q. W. Yin, C. S. Gong, Z. J. Tu, H. C. Lei, T. Dong, and N. L. Wang, Phys. Rev. B **106**, 205109 (2022).
[17] Y. Xu, Z. Ni, Y. Liu, B. R. Ortiz, Q. Deng, S. D. Wilson, B. Yan, L. Balents, and L. Wu, Nat. Phys. **18**, 1470 (2022).
[18] C. Guo, C. Putzke, S. Konyzheva, X. Huang, M. Gutierrez-Amigo, I. Errea, D. Chen, M. G. Vergniory, C. Felser, M. H. Fischer, T. Neupert, and P. J. W. Moll, Nature (London) **611**, 461 (2022).
[19] Y. Xing, S. Bae, E. Ritz, F. Yang, T. Birol, A. N. Capa Salinas, B. R. Ortiz, S. D. Wilson, Z. Wang, R. M. Fernandes, and V. Madhavan, Nature (London) **631**, 60 (2024).
[20] K. Y. Chen, N. N. Wang, Q. W. Yin, Y. H. Gu, K. Jiang, Z. J. Tu, C. S. Gong, Y. Uwatoko, J. P. Sun, H. C. Lei, J. P. Hu, and J.-G. Cheng, Phys. Rev. Lett. **126**, 247001 (2021).
[21] Z. Zhang, Z. Chen, Y. Zhou, Y. Yuan, S. Wang, J. Wang, H. Yang, C. An, L. Zhang, X. Zhu, Y. Zhou, X. Chen, J. Zhou, and Z. Yang, Phys. Rev. B **103**, 224513 (2021).
[22] X. Chen, X. Zhan, X. Wang, J. Deng, X.-B. Liu, X. Chen, J.-G. Guo, and X. Chen, Chin. Phys. Lett. **38**, 057402 (2021).
[23] Y. Song, T. Ying, X. Chen, X. Han, X. Wu, A. P. Schnyder, Y. Huang, J.-g. Guo, and X. Chen, Phys. Rev. Lett. **127**, 237001 (2021).
[24] Y. M. Oey, B. R. Ortiz, F. Kaboudvand, J. Frassineti, E. Garcia, R. Cong, S. Sanna, V. F. Mitrović, R. Seshadri, and S. D. Wilson, Phys. Rev. Mater. **6**, L041801 (2022).
[25] Y. Liu, Y. Wang, Y. Cai, Z. Hao, X.-M. Ma, L. Wang, C. Liu, J. Chen, L. Zhou, J. Wang, S. Wang, H. He, Y. Liu, S. Cui, B. Huang, J. Wang, C. Chen, and J.-W. Mei, Phys. Rev. Mater. **7**, 064801 (2023).
[26] X. Feng, K. Jiang, Z. Wang, and J. Hu, Sci. Bull. **66**, 1384 (2021).
[27] M. M. Denner, R. Thomale, and T. Neupert, Phys. Rev. Lett. **127**, 217601 (2021).
[28] Y.-P. Lin and R. M. Nandkishore, Phys. Rev. B **104**, 045122 (2021).
[29] T. Park, M. Ye, and L. Balents, Phys. Rev. B **104**, 035142 (2021).
[30] C. M. Varma, Phys. Rev. B **55**, 14554 (1997).
[31] S. Chakravarty, R. B. Laughlin, D. K. Morr, and C. Nayak, Phys. Rev. B **63**, 094503 (2001).
[32] C. M. Varma, Phys. Rev. Lett. **83**, 3538 (1999).
[33] F. D. M. Haldane, Phys. Rev. Lett. **61**, 2015 (1988).
[34] S. Raghu, X.-L. Qi, C. Honerkamp, and S.-C. Zhang, Phys. Rev. Lett. **100**, 156401 (2008).
[35] A. Macridin, M. Jarrell, and T. Maier, Phys. Rev. B **70**, 113105 (2004).
[36] F. F. Assaad, Phys. Rev. B **71**, 075103 (2005).
[37] C. Weber, A. Läuchli, F. Mila, and T. Giamarchi, Phys. Rev. Lett. **102**, 017005 (2009).
[38] M. Greiter and R. Thomale, Phys. Rev. Lett. **99**, 027005 (2007).
[39] C. Weber, T. Giamarchi, and C. M. Varma, Phys. Rev. Lett. **112**, 117001 (2014).
[40] N. A. García-Martínez, A. G. Grushin, T. Neupert, B. Valenzuela, and E. V. Castro, Phys. Rev. B **88**, 245123 (2013).
[41] M. Daghofer and M. Hohenadler, Phys. Rev. B **89**, 035103 (2014).
[42] J. Motruk, A. G. Grushin, F. de Juan, and F. Pollmann, Phys. Rev. B **92**, 085147 (2015).
[43] S. Capponi and A. M. Läuchli, Phys. Rev. B **92**, 085146 (2015).
[44] D. D. Scherer, M. M. Scherer, and C. Honerkamp, Phys. Rev. B **92**, 155137 (2015).

[45] M. L. Kiesel and R. Thomale, Phys. Rev. B **86**, 121105(R) (2012).
[46] X. Wu, T. Schwemmer, T. Müller, A. Consiglio, G. Sangiovanni, D. Di Sante, Y. Iqbal, W. Hanke, A. P. Schnyder, M. M. Denner, M. H. Fischer, T. Neupert, and R. Thomale, Phys. Rev. Lett. **127**, 177001 (2021).
[47] M. L. Kiesel, C. Platt, and R. Thomale, Phys. Rev. Lett. **110**, 126405 (2013).
[48] S.-L. Yu and J.-X. Li, Phys. Rev. B **85**, 144402 (2012).
[49] W.-S. Wang, Z.-Z. Li, Y.-Y. Xiang, and Q.-H. Wang, Phys. Rev. B **87**, 115135 (2013).
[50] F. Ferrari, F. Becca, and R. Valentí, Phys. Rev. B **106**, L081107 (2022).
[51] J.-W. Dong, Z. Wang, and S. Zhou, Phys. Rev. B **107**, 045127 (2023).
[52] R. Fu, J. Zhan, M. Dürrnagel, H. Hohmann, R. Thomale, J. Hu, Z. Wang, S. Zhou, and X. Wu, Natl. Sci. Rev. **12**, nwaf414 (2025).
[53] J. Wen, A. Rüegg, C.-C. Joseph Wang, and G. A. Fiete, Phys. Rev. B **82**, 075125 (2010).
[54] See Supplemental Material at http://link.aps.org/supplemental/10.1103/5vyy-rj6v for details of the FRG methods employed, the Ginzburg-Landau analysis, and the physical properties of LCO, as well as its realizations in a spinful model with Zeeman splitting. Supplemental Material also includes Refs. [55–61].
[55] W.-S. Wang, Y.-Y. Xiang, Q.-H. Wang, F. Wang, F. Yang, and D.-H. Lee, Phys. Rev. B **85**, 035414 (2012).
[56] J. Lichtenstein, D. Sánchez de la Peña, D. Rohe, E. Di Napoli, C. Honerkamp, and S. A. Maier, Comput. Phys. Commun. **213**, 100 (2017).
[57] C. Husemann and M. Salmhofer, Phys. Rev. B **79**, 195125 (2009).
[58] C. Honerkamp and M. Salmhofer, Phys. Rev. B **64**, 184516 (2001).
[59] R. Nandkishore, G.-W. Chern, and A. V. Chubukov, Phys. Rev. Lett. **108**, 227204 (2012).
[60] D. Xiao, M.-C. Chang, and Q. Niu, Rev. Mod. Phys. **82**, 1959 (2010).
[61] M. Sigrist and K. Ueda, Rev. Mod. Phys. **63**, 239 (1991).
[62] W. Metzner, M. Salmhofer, C. Honerkamp, V. Meden, and K. Schönhammer, Rev. Mod. Phys. **84**, 299 (2012).
[63] C. Platt, W. Hanke, and R. Thomale, Adv. Phys. **62**, 453 (2013).
[64] J. Beyer, J. B. Hauck, and L. Klebl, Eur. Phys. J. B **95**, 65 (2022).
[65] S.-J. O, Y.-H. Kim, O.-G. Pak, K.-H. Jong, C.-W. Ri, and H.-C. Pak, Phys. Rev. B **103**, 235150 (2021).
[66] N. Gneist, D. Kiese, R. Henkel, R. Thomale, L. Classen, and M. M. Scherer, Eur. Phys. J. B **95**, 157 (2022).
[67] J. B. Profe, L. Klebl, F. Grandi, H. Hohmann, M. Dürrnagel, T. Schwemmer, R. Thomale, and D. M. Kennes, Phys. Rev. Res. **6**, 043078 (2024).
[68] R. Tazai, Y. Yamakawa, and H. Kontani, Nat. Commun. **14**, 7845 (2023).
[69] T. Schwemmer, H. Hohmann, M. Dürrnagel, J. Potten, J. Beyer, S. Rachel, Y.-M. Wu, S. Raghu, T. Müller, W. Hanke, and R. Thomale, Phys. Rev. B **110**, 024501 (2024).
[70] Y. Hu, X. Wu, B. R. Ortiz, S. Ju, X. Han, J. Ma, N. C. Plumb, M. Radovic, R. Thomale, S. D. Wilson, A. P. Schnyder, and M. Shi, Nat. Commun. **13**, 2220 (2022).
[71] M. Kang, S. Fang, J.-K. Kim, B. R. Ortiz, S. H. Ryu, J. Kim, J. Yoo, G. Sangiovanni, D. Di Sante, B.-G. Park, C. Jozwiak, A. Bostwick, E. Rotenberg, E. Kaxiras, S. D. Wilson, J.-H. Park, and R. Comin, Nat. Phys. **18**, 301 (2022).
[72] Y. Jiang, H. Hu, D. C ălugăru, C. Felser, S. Blanco-Canosa, H. Weng, Y. Xu, and B. A. Bernevig, Phys. Rev. B **111**, 125163 (2025).
[73] H. Tan, Y. Liu, Z. Wang, and B. Yan, Phys. Rev. Lett. **127**, 046401 (2021).
[74] M. Gutierrez-Amigo, D. Dangic, C. Guo, C. Felser, P. J. W. Moll, M. G. Vergniory, and I. Errea, Commun. Mater. **5**, 234 (2024).
[75] H. Li, Y. B. Kim, and H.-Y. Kee, Phys. Rev. Lett. **132**, 146501 (2024).
[76] S. Zhou and Z. Wang, Nat. Commun. **13**, 7288 (2022).